Front. Struct. Civ. Eng. 2021, 15(3): 609–622
https://doi.org/10.1007/s11709-021-0724-x

RESEARCH ARTICLE

Modeling limit force capacities of high force to volume lead extrusion dampers

V. VISHNUPRIYA[a,b*], Geoffrey. W. RODGERS[a,b], J. Geoffrey CHASE[a]

[a] *Department of Mechanical Engineering, University of Canterbury, Christchurch 8140, New Zealand*

[b] *QuakeCoRE NZ Centre for Earthquake Resilience, Christchurch 8041, New Zealand*

[*] *Corresponding author. E-mail: 282vishnupriya@gmail.com*

ABSTRACT Lead extrusion dampers are supplemental energy-dissipation devices that are used to mitigate seismic structural damage. Small volumetric sizes and high force capacities define high-force-to-volume (HF2V) devices, which can absorb significant response energy without sacrificial damage. However, the design of such devices for specific force capacities has proven difficult based on the complexities of their internal reaction mechanisms, leading to the adoption of empirical approaches. This study developed upper- and lower-bound force capacity estimates from analytical mechanics based on direct and indirect metal extrusion for guiding design. The derived equations are strictly functions of HF2V device geometric parameters, lead material properties, and extrusion mechanics. The upper-bound estimates from direct and indirect extrusion are denoted as ($F_{UB,1}$, $F_{UB,2}$) and ($F_{UB,3}$, $F_{UB,4}$), respectively, and the lower-bound estimates are denoted as (F_{LB}, $F_{LB,1}$) based on the combination of extrusion and friction forces. The proposed models were validated by comparing the predicted bounds to experimental force capacity data from 15 experimental HF2V device tests. The experimental device forces all lie above the lower-bound estimates (F_{LB}, $F_{LB,1}$) and below the upper-bound estimates ($F_{UB,1}$, $F_{UB,2}$, $F_{UB,4}$). Overall, the (F_{LB}, $F_{UB,2}$) pair provides wider bounds and the ($F_{LB,1}$, $F_{UB,4}/F_{UB,1}$) pair provides narrower bounds. The ($F_{LB,1}$, $F_{UB,1}$) pair has a mean lower-bound gap of 36%, meaning the lower bound was 74% of the actual device force on average. The mean upper-bound gap was 33%. The bulge area and cylinder diameter of HF2V devices are key parameters affecting device forces. These relatively tight bounds provide useful mechanics-based predictive design guides for ensuring that device forces are within the targeted design range after manufacturing.

KEYWORDS extrusion, lead dampers, upper and lower bound, analytical modelling, limit force

1 Introduction

Earthquakes are episodic events in seismically active areas that represent a significant natural hazard. However, there are no reliable methods for forecasting of the strength or occurrence of earthquakes [1–3]. The effects of a seismic event may be severe, leaving lasting socioeconomic and psychological impacts in affected areas. The overall strength of a structure can be enhanced by using passive supplemental dampers to mitigate building responses during an earthquake.

Lead extrusion dampers are supplemental energy devices that utilize the hysteretic properties of lead to absorb response energy and reduce the responses of structures to earthquake loading. The first application of lead extrusion dampers was in the Wellington Motorway Overbridges [4]. Dissipative forces are generated when the lead working material is extruded between a wall and bulged shaft as the shaft is displaced by structural responses to ground excitations. High-force-to-volume (HF2V) devices are lead extrusion dampers designed to provide higher force capacities with smaller sizes [5–9]. The design of HF2V devices is an important aspect of structural applications or retrofitting. The accurate prediction of the HF2V force capacity in the design phase allows for the appropriate selection of devices that are suitable for structural damping and target design requirements. However, effective design tools for estimating the seismic resistive force capacities of HF2V devices are limited

Article history: Received Jul 5, 2020; Accepted Nov 19, 2020

[10,11]. Recently, enhanced equations have been developed to match device mechanisms directly and provide reliable predictions of device force behavior [12,13].

For the seismic protection of large structures, a large number of HF2V devices of varying sizes and force capacities may be required according to the structural design requirements [14–17]. Obtaining the minimum and maximum force limits of HF2V devices is necessary for achieving the desired operational range of the devices during plastic deformation. The identification of device parameters that directly influence damping forces is valuable for future HF2V design selection.

2 Direct and indirect extrusion analogies

Extrusion is a forming process in which a working material is forced between dies by an external load. Generally, for direct extrusion processes, a ram moves forward to push a metal billet through a die orifice at room temperature, thereby extruding the metal in the same direction as the ram. The metal is sheared and compressed between the dies to produce the desired metal parts. Typical direct extrusion examples are presented in Fig. 1(a).

For indirect metal forming processes, a stamp head is forced through the working material by applying a force on the stamp, which is useful for forming hollow tubes. Unlike direct extrusion, the entire workpiece is not displaced by forcing the ram to pass through an orifice. The stamp pushes through the workpiece such that the working material compresses and shears in the direction opposite to the direction of displacement of the stamp, as shown in Fig. 1(b).

The extrusion process in an HF2V device, which is illustrated in Fig. 1(c), is a closed container operation in which a working material can be repeatedly extruded via shaft displacement. In a pre-stressed HF2V device, lead is plastically deformed during extrusion and regains its mechanical properties through recrystallization behind the bulge [18]. It is then forced to flow against the shaft behind the bulge [19]. The working material remains within the containing cylinder following extrusion and there are no changes in the overall configuration of the working material in an HF2V device, unlike in metal-forming extrusion processes. Although the reversible extrusion process used within these devices does not strictly match conventional extrusion processes, close analogies exist between these processes. The bulge in an HF2V device is analogous to the stamp head in an indirect extrusion process and to the die in a direct extrusion process. The functions of the bulge, stamp head, and die are all to deform the metal during the extrusion process. Compression and shear forces are produced by the deformation of the metal and friction between the metal and moving parts in both processes.

The interaction of the working material (lead) with the

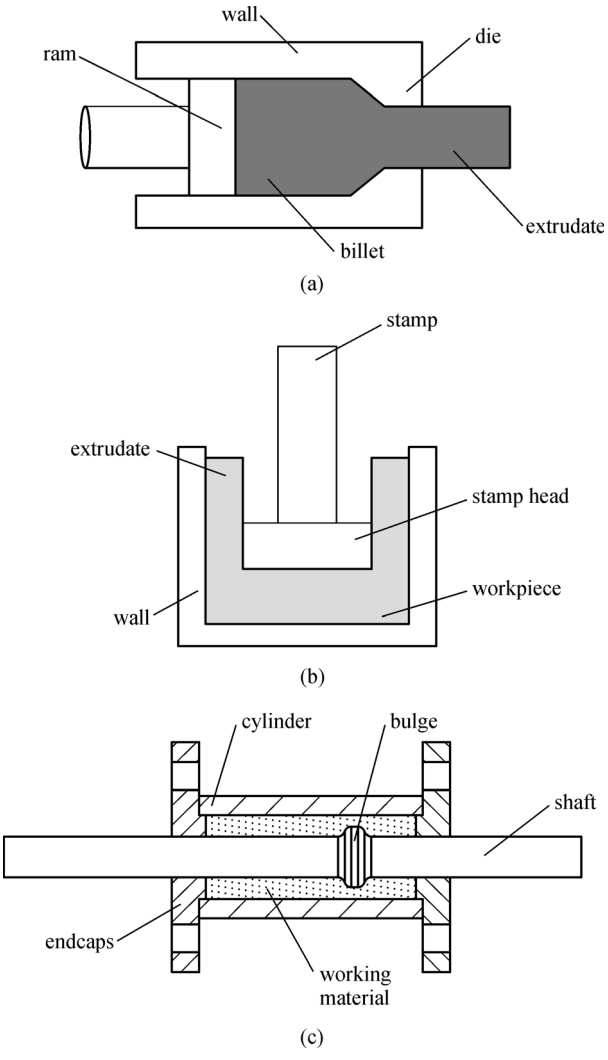

Fig. 1 (a) Direct extrusion; (b) indirect extrusion; (c) HF2V device.

cylinder walls of an HF2V device is uncertain because there is no simple methodology for observing the actual flow of lead during shaft displacement in a device. Due to the ambiguity of the forces stemming from wall friction, two assumptions are considered in this study.

Assumption 1: Intermetallic shear occurs in lead during shaft displacement and lead only shears along the shaft during displacement, meaning the lead along the wall is not displaced [20]. Therefore, there are no frictional forces from the cylinder walls and only internal shearing within the lead.

Assumption 2: Friction forces are generated by the flow of lead along the cylinder wall during shaft displacement, thereby contributing to overall HF2V device forces.

2.1 Limit loads

Based on the inherent complexity of the extrusion process, the exact prediction of extrusion forces can be difficult.

Instead, most studies seek to approximate the upper and lower limits of extrusion forces [21–23]. Upper-bound (UB) theorems estimate maximum forces based on yield criteria and geometric self-consistency. Lower-bound (LB) theorems determine the minimum forces produced while ignoring geometric self-consistency [23,24].

The plain strain theory can be applied to metal forming processes with axisymmetric geometry for predicting approximate extrusion forces [25–28]. UB forces can be estimated using the slip line field theory, which is a graphical method for determining the working load during metal deformation that assumes that polycrystalline metals always slip in the direction of maximum shear stress. Therefore, the slip line field theory provides a graphical representation of the direction of maximum shear force at every point in a deforming body [22]. However, the construction of a slip line field and hodograph for force estimation is complex and unreliable if the slip line fields are inaccurate or not scaled properly [25,27,29,30].

Several generalized models are available for UB approximations of axisymmetric direct and indirect extrusion forces [31–37]. However, only a few models are based on geometric parameters and are influenced by the frictional conditions involved in extrusion [38]. Because HF2V device operation is based on extrusion, device parameters are matched to direct and indirect metal extrusion processes to obtain UB and LB force capacities for such devices, providing insights into their operating mechanics and design.

2.2 Direct-extrusion-based high-force-to-volume upper-bound modeling

Our UB models were developed based on existing UB models for extrusion UB force calculations. A simplified and efficient UB extrusion solution for lead and aluminum alloys is considered in this analysis based on a simplified direct analogy between an extrusion model and HF2V device operation [31–33]. We consider a generalized UB model independent of velocity fields and slip line fields [25], which is defined as

$$F_{\mathrm{d}} = 2k\left[4\mu\left(\frac{H}{D}+\frac{h}{d}\right)+\left(\frac{\mu}{\sin\alpha}+1\right)\ln\frac{D^2}{d^2}\right]\frac{\pi D^2}{4}, \quad (1)$$

where k is the maximum tangential stress, D is the billet container diameter, H is the length of the billet in the container, d is the diameter of the extruded metal, h is the length of the die land, μ is the coefficient of friction, and α is the die angle, as shown in Fig. 2(a).

For direct extrusion comparisons to an HF2V device, geometric device parameters are mapped onto HF2V devices for UB modeling, as shown in Fig. 2(b), and the following initial assumptions are adopted.

a) The bulges of the HF2V damper are assumed to be on the walls of the device, as shown in Fig. 2(b), and it is assumed that this equivalent analogy will yield the same forces.

b) Additionally, the friction from a no-bulge shaft is considered for modeling.

c) The ram moves and the lead is extruded between the two bulges on the walls, generating both extrusion and friction forces.

d) Friction between the endplates is neglected.

According to Fig. 2(b), Eq. (1) can be modified to match the geometric parameters defining HF2V devices. The additional friction force (F_{f}) from the shaft is added to the modified UB, which is then defined as

$$F_{\mathrm{UB,direct}} = 2Y_{\mathrm{o}}\frac{\pi(D_{\mathrm{cyl}}-D_{\mathrm{sh}})^2}{4}\left[4\mu\left(\frac{L_{\mathrm{cyl}}-L_{\mathrm{blg}}}{D_{\mathrm{cyl}}-D_{\mathrm{sh}}}+\frac{L_{\mathrm{flat\ blg}}}{D_{\mathrm{cyl}}-D_{\mathrm{blg}}}\right)+\left(\frac{\mu}{\sin\alpha}+1\right)\ln\left(\frac{D_{\mathrm{cyl}}-D_{\mathrm{sh}}}{D_{\mathrm{cyl}}-D_{\mathrm{blg}}}\right)^2\right]+F_{\mathrm{f}}, \quad (2)$$

where Y_{o} is the yield strength of the lead, μ is the coefficient of friction between the lead and steel shaft surface, L_{cyl} is the length of the cylinder, L_{blg} is the length of the bulge, $L_{\mathrm{flat\ blg}}$ is the length of the flat surface of the bulge, which is similar to the die land in direct extrusion, D_{cyl} is the cylinder diameter, D_{blg} is the bulge diameter, D_{sh} is the shaft diameter, and α is the bulge angle. All of the HF2V device geometric parameters used in Eq. (2) are illustrated in Fig. 3.

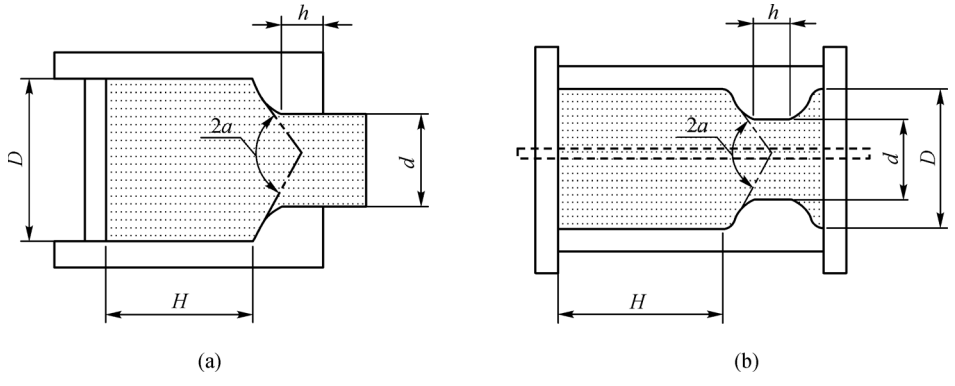

Fig. 2 (a) Direct extrusion parameters from Eq. (1) and (b) direct extrusion geometry mapping to an HF2V device.

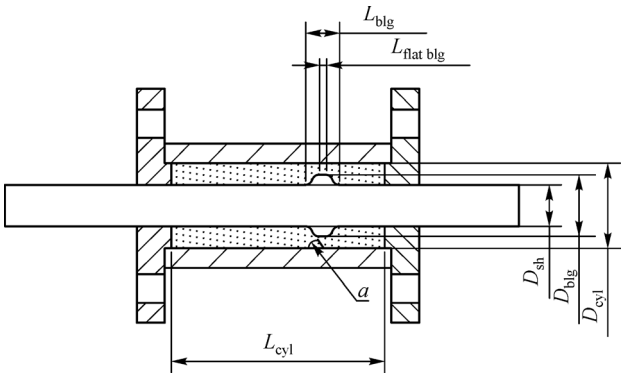

Fig. 3 HF2V lead extrusion damper parameters.

During shaft displacement, large deformations occur in the lead working material based on shearing caused by the bulge as it passes through the lead working material. To obtain the maximum possible HF2V device force for calculating a UB, the yield strength (Y_o) of the material is considered instead of the maximum tangential stress (k). The value of F_f and the friction coefficient considered for modeling are discussed in detail in Section 2.5.

2.2.1 Upper bound model 1 ($F_{UB,1}$)

The friction forces produced in HF2V devices between the cylinder walls and lead are neglected in this model according to Assumption 1. However, the friction forces generated by friction between the lead and shaft (F_f) are captured in this model and defined as

$$F_{UB,1} = 2Y_o \frac{\pi(D_{cyl}-D_{sh})^2}{4}\left[4\mu\left(\frac{L_{cyl}-L_{blg}}{D_{cyl}-D_{sh}} + \frac{L_{flat\ blg}}{D_{cyl}-D_{blg}}\right)\ln\left(\frac{D_{cyl}-D_{sh}}{D_{cyl}-D_{blg}}\right)^2\right] + F_f, \quad (3)$$

where F_f is the friction of lead along the entire shaft, as defined in Section 2.5. Because the friction forces generated at the cylinder walls are neglected, the minimum friction coefficient can be considered to be 0.05 between the lead and walls for the calculation of $F_{UB,1}$ [39,40]. The friction coefficient is μ = 0.25 and is assumed to be constant at all points of interaction between the lead and shaft surface [41,42].

2.2.2 Upper bound model 2 ($F_{UB,2}$)

According to Assumption 2, the $F_{UB,2}$ model accounts for the friction forces from lead-wall interactions [12,13]. The friction coefficient for the lead-wall and lead-shaft interactions is 0.25, similar to Eq. (1), for $F_{UB,2}$ modeling [42]. The modified UB equation under Assumption 2 is defined as

$$F_{UB,2} = 2Y_o \frac{\pi(D_{cyl}-D_{sh})^2}{4}\left[4\mu\left(\frac{L_{cyl}-L_{blg}}{D_{cyl}-D_{sh}} + \frac{L_{flat\ blg}}{D_{cyl}-D_{blg}}\right)\ln\left(\frac{D_{cyl}-D_{sh}}{D_{cyl}-D_{blg}}\right)^2\right] + F_{f\_sh}, \quad (4)$$

where F_{f_sh} is the friction force generated by the non-bulged shaft, as defined in Section 2.5. The friction forces along the bulged shaft are captured in this model.

2.3 Indirect-extrusion-based high-force-to-volume upper-bound modeling

The overall geometry of indirect extrusion is similar to that of the HF2V devices shown in Fig. 4. The stamp head compresses and shears the metal and passes through the workpiece, similar to the bulged shaft in HF2V devices. The shaft bulge is analogous to the stamp and the container wall and workpiece are analogous to the cylinder walls and working material (lead), respectively. However, the extruded workpiece does not flow over the shaft behind the stamp head. In typical indirect extrusion, the extruded workpiece retains the die geometry.

A constitutive approach is considered for indirect extrusion force modeling, where the sum of forces dissipated during the extrusion process is calculated [30,34,43]. The forces produced by indirect extrusion stem from friction between the workpiece and stamp (F_p), workpiece and cylinder wall (F_m), compression of the workpiece (F_r), and deformation of the workpiece (F_{def}) [34], and are defined as follows:

$$F_i = \left(8\mu k \cdot \frac{h_p}{d}\frac{D^2}{D^2-d^2}\cdot\frac{\pi d^2}{4}\right)_{F_p} + \left(8\mu k D \cdot \frac{h_m + \frac{h}{2}}{D^2-d^2}\cdot\frac{D^2}{d^2}\cdot\frac{\pi d^2}{4}\right)_{F_m} + \left[2k\cdot\frac{\pi d^2}{4}\cdot\left(1+\frac{\mu d}{H}\right)\right]_{F_r} + \left(2k\cdot\frac{D^2}{d^2}\cdot\frac{\pi d^2}{4}\ln\frac{D^2}{D^2-d^2}\right)_{F_p}, \quad (5)$$

where D is the diameter of the container, d is the diameter of the stamp head, h_p is the height of the stamp, h_m is the length of the extruded workpiece behind the stamp, H is the height of the non-deformed workpiece, and h is defined as follows:

$$h = \frac{D+d}{2}\frac{\sqrt{D^2-d^2}}{d}. \quad (6)$$

These geometric parameters for indirect extrusion can be mapped to HF2V devices for modeling UB forces, as shown in Fig. 4.

By using the indirect extrusion modeling methodology, the UB limits of the total HF2V device forces can be calculated from the sum of the UB limits of the friction forces generated by the lead-bulge ($F_{\mathrm{f\_blg}}$), lead-shaft ($F_{\mathrm{f\_sh}}$), and lead-wall ($F_{\mathrm{f\_wall}}$) interactions, as well as the compression forces (F_{comp}), deformation forces (F_{def}), and extrusion forces (F_{ext}) stemming from area reduction, by adapting Eq. (5) [34]. The total HF2V UB force can be calculated as follows:

$$F_{\mathrm{UB,indirect}} = F_{\mathrm{comp}} + F_{\mathrm{def}} + F_{\mathrm{f\_blg}} + F_{\mathrm{f\_sh}} + F_{\mathrm{f\_wall}} + F_{\mathrm{ext}}. \tag{7}$$

The expression for the compressive forces of HF2V devices is defined as follows:

$$F_{\mathrm{comp}} = 2Y_{\mathrm{o}}\left(1 + \mu\frac{D_{\mathrm{blg}} - D_{\mathrm{sh}}}{L_{\mathrm{cyl}} - L_{\mathrm{blg}}}\right)\frac{\pi(D_{\mathrm{blg}} - D_{\mathrm{sh}})^2}{4}. \tag{8}$$

The deformation forces are defined as follows:

$$F_{\mathrm{def}} = 2Y_{\mathrm{o}}\frac{D_{\mathrm{cyl}}^2}{d^2}\frac{\pi d^2}{4}\ln\frac{D_{\mathrm{cyl}}^2}{D_{\mathrm{cyl}}^2 - (D_{\mathrm{blg}} - D_{\mathrm{sh}})^2}. \tag{9}$$

The force generated by the friction between the bulged shaft and working material is calculated as follows:

$$F_{\mathrm{f\_blg}} = 8\mu Y_{\mathrm{o}}\frac{(L_{\mathrm{blg}})}{D_{\mathrm{blg}} - D_{\mathrm{sh}}}\frac{\pi(D_{\mathrm{blg}} - D_{\mathrm{sh}})^2}{4}\frac{D_{\mathrm{cyl}}^2}{D_{\mathrm{cyl}}^2 - (D_{\mathrm{blg}} - D_{\mathrm{sh}})^2}. \tag{10}$$

The working material flows against the wall, creating friction forces between the wall and working material, which are defined as follows:

$$F_{\mathrm{f\_wall}} = 8\mu Y_{\mathrm{o}}\frac{L_{\mathrm{blg}} + h/2}{D_{\mathrm{cyl}}^2 - (D_{\mathrm{blg}} - D_{\mathrm{sh}})^2}\frac{\pi(D_{\mathrm{blg}} - D_{\mathrm{sh}})^2}{4}\frac{D_{\mathrm{cyl}}^2}{D_{\mathrm{cyl}}^2 - (D_{\mathrm{blg}} - D_{\mathrm{sh}})^2}, \tag{11}$$

where h is defined as

$$h = \frac{D_{\mathrm{cyl}} + (D_{\mathrm{blg}} - D_{\mathrm{sh}})}{2} + \frac{\sqrt{D_{\mathrm{cyl}}^2 - D_{\mathrm{sh}}^2}}{2}, \tag{12}$$

in accordance with the indirect extrusion force calculated using Eq. (6) [34].

The shaft friction force ($F_{\mathrm{f\_sh}}$) can be calculated as shown in Section 2.5. The extrusion forces (F_{ext}) can be estimated using the equations derived in Section 2.4.

2.3.1 Upper-bound model 3 ($F_{\mathrm{UB,3}}$)

UB force calculation using the indirect extrusion process with the assumption of no friction at the lead-wall boundary (Assumption 1) yields $F_{\mathrm{UB,3}}$, which considers the friction forces generated by the interaction of the lead and shaft. The wall friction forces are neglected in Eq. (7) to obtain the HF2V device UB force, namely $F_{\mathrm{UB,3}}$, which is defined as

$$F_{\mathrm{UB,3}} = F_{\mathrm{comp}} + F_{\mathrm{def}} + F_{\mathrm{f\_blg}} + F_{\mathrm{f\_sh}} + F_{\mathrm{ext}}. \tag{13}$$

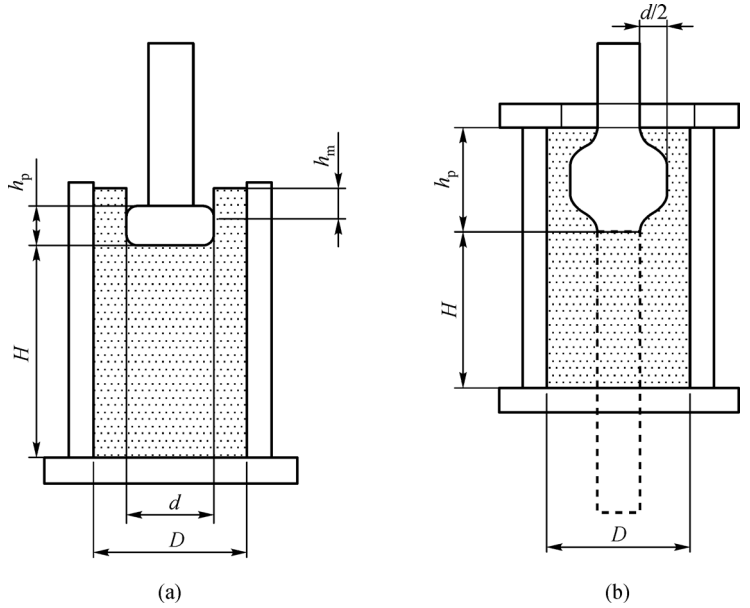

Fig. 4 (a) Indirect extrusion parts and (b) geometric mapping of parameters onto HF2V devices.

2.3.2 Upper-bound model 4 ($F_{UB,4}$)

According to Assumption 2, the working material flows against the direction of motion relative to the wall, generating friction forces between the wall and lead, which are calculated using Eq. (11). The modified UB force model $F_{UB,4}$ considering the wall friction forces in HF2V devices is defined as follows:

$$F_{UB,4} = F_{comp} + F_{def} + F_{f\_blg} + F_{f\_sh} + F_{ext} + F_{f\_wall}. \quad (14)$$

2.4 Lower-bound equation ($F_{LB,1}$)

LB extrusion forces can be estimated based on the work models used to obtain metalworking loads, which assume homogenous deformation and zero friction, as follows [25,43,44]:

$$F_{LB} = A_o Y_o \ln\frac{A_o}{A_f}, \quad (15)$$

where Y_o is the yield stress, A_o is the area of the lead before extrusion, and A_f is the area of the area after extrusion, which is defined for HF2V devices as illustrated in Fig. 3.

$$A_o = \pi\frac{(D_{cyl} - D_{sh})^2}{4};\ A_f = \pi\frac{(D_{cyl} - D_{blg})^2}{4}. \quad (16)$$

This model assumes ideal deformation with no friction and no redundant work [45]. Based on this assumption, this model can be used to estimate the extrusion forces in a device when the friction between the steel parts and lead is negligible. This condition can occur if surfaces are lubricated. Ignoring these terms is an appropriate simplifying assumption when calculating an LB. Therefore, $F_{LB,1} = F_{ext}$.

2.4.1 Modified lower-bound equation ($F_{LB,2}$)

In previous studies, HF2V forces have been obtained in terms of extrusion forces and friction forces [12,13]. Hence, the force required to overcome friction and achieve shaft displacement must be considered for LB modeling. The overall LB force developed in an HF2V damper can be obtained by adding F_f to Eq. (15) as follows:

$$F_{LB,1} = A_o Y_o \ln\frac{A_o}{A_f} + F_f. \quad (17)$$

2.5 Friction force (F_f) modeling

Frictional stresses are a function of the yield stress, temperature, strain, velocity, and area of contact. Depending on these factors, many advanced frictional models have been proposed for extrusion [46–50]. The Coulomb friction model is the earliest and most frequently used friction model for extrusion. It is only dependent on the load and direction of velocity, and estimates the dynamic friction forces generated by sliding [51]. A Coulomb-friction-based model is used to calculate the friction forces from the lead-shaft interface [49,52–54] as follows:

$$F_F = m\pi DL\frac{Y_o}{\sqrt{3}}. \quad (18)$$

The von Mises–Coulomb friction model is adopted and modified in Eq. (18). This model assumes that shear stresses are proportional to normal forces [52–55]. However, a true estimate of the shear forces in a device can be derived only if the actual area of contact between the lead and shaft/container is known [46].

The length of the shaft in contact with the lead is equal to the length of the cylinder (L_{cyl}). Therefore, the frictional force component for the entire shaft is defined as follows:

$$F_f = m\pi D_{sh}\frac{Y_o}{\sqrt{3}}L_{cyl}. \quad (19)$$

The length of the bulge, denoted as L_{blg}, is excluded from Eq. (4) because the friction contribution of the bulge is already captured. The frictional force component is defined as follows:

$$F_{f\_sh} = m\pi D_{sh}\frac{Y_o}{\sqrt{3}}(L_{cyl} - L_{blg}). \quad (20)$$

2.6 Summary of upper-bound and lower-bound equations

The final UB and LB equations are summarized in Table 1.

2.7 Analysis

The UB and LB models listed in Table 1 were applied to 15 HF2V lead extrusion dampers whose experimental test data are available from previous studies [5,56,57]. These 15 devices are listed in Table 2. The following assumptions were made for UB analysis.

i) The friction coefficient (μ) = 0.25 and is assumed to be constant at all points of interaction between the lead and shaft surfaces.

ii) The forces of compression behind the bulge slope following extrusion are neglected.

iii) The velocity of the shaft relative to the outer casing is assumed to be 0.5 mm/s.

iv) The effects of temperature are not considered in this analysis.

For LB analysis, the temperature was assumed to be 20°C. The yield strength was considered to be twice the average flow stress ($\overline{Y}$) [45] and defined as follows:

$$Y_o = 2\overline{Y}. \quad (21)$$

The flow stress is the stress value at which the metal

Table 1 HF2V UB and LB equations used for analysis

equation description	UB and LB equations
$F_{UB,1}$: UB without wall friction from direct extrusion	$F_{\mathrm{UB},1}=2Y_{\mathrm{o}}\frac{\pi(D_{\mathrm{cyl}}-D_{\mathrm{sh}})^2}{4}\left[4\mu\left(\frac{L_{\mathrm{cyl}}-L_{\mathrm{blg}}}{D_{\mathrm{cyl}}-D_{\mathrm{sh}}}+\frac{L_{\mathrm{flat\ blg}}}{D_{\mathrm{cyl}}-D_{\mathrm{blg}}}\right)\ln\left(\frac{D_{\mathrm{cyl}}-D_{\mathrm{sh}}}{D_{\mathrm{cyl}}-D_{\mathrm{blg}}}\right)^2\right]+m\pi D_{\mathrm{sh}}\frac{Y_{\mathrm{o}}}{\sqrt{3}}L_{\mathrm{cyl}}$
$F_{UB,2}$: UB with wall friction from direct extrusion	$F_{\mathrm{UB},2}=2Y_{\mathrm{o}}\frac{\pi(D_{\mathrm{cyl}}-D_{\mathrm{sh}})^2}{4}\left[4\mu\left(\frac{L_{\mathrm{cyl}}-L_{\mathrm{blg}}}{D_{\mathrm{cyl}}-D_{\mathrm{sh}}}+\frac{L_{\mathrm{flat\ blg}}}{D_{\mathrm{cyl}}-D_{\mathrm{blg}}}\right)\ln\left(\frac{D_{\mathrm{cyl}}-D_{\mathrm{sh}}}{D_{\mathrm{cyl}}-D_{\mathrm{blg}}}\right)^2\right]+m\pi D_{\mathrm{sh}}\frac{Y_{\mathrm{o}}}{\sqrt{3}}(L_{\mathrm{cyl}}-L_{\mathrm{blg}})$
$F_{UB,3}$: UB without wall friction from indirect extrusion	$F_{\mathrm{UB},3}=Y_{\mathrm{o}}\left[2\left(1+\mu\frac{D_{\mathrm{blg}}-D_{\mathrm{sh}}}{L_{\mathrm{cyl}}-L_{\mathrm{blg}}}\right)\frac{\pi(D_{\mathrm{blg}}-D_{\mathrm{sh}})^2}{4}+2\frac{D_{\mathrm{cyl}}^2}{d^2}\frac{\pi d^2}{4}\ln\frac{D_{\mathrm{cyl}}^2}{D_{\mathrm{cyl}}^2-(D_{\mathrm{blg}}-D_{\mathrm{sh}})^2}+8\mu\frac{L_{\mathrm{blg}}}{D_{\mathrm{blg}}-D_{\mathrm{sh}}}\frac{\pi(D_{\mathrm{blg}}-D_{\mathrm{sh}})^2}{4}\frac{D_{\mathrm{cyl}}^2}{D_{\mathrm{cyl}}^2-(D_{\mathrm{blg}}-D_{\mathrm{sh}})^2}+A_{\mathrm{o}}\ln\frac{A_{\mathrm{o}}}{A_{\mathrm{f}}}+m\pi D_{\mathrm{sh}}\frac{L_{\mathrm{cyl}}}{\sqrt{3}}\right]$
$F_{UB,4}$: UB with wall friction from indirect extrusion	$F_{\mathrm{UB},4}=Y_{\mathrm{o}}\left[2\left(1+\mu\frac{D_{\mathrm{blg}}-D_{\mathrm{sh}}}{L_{\mathrm{cyl}}-L_{\mathrm{blg}}}\right)\frac{\pi(D_{\mathrm{blg}}-D_{\mathrm{sh}})^2}{4}+2\frac{D_{\mathrm{cyl}}^2}{d^2}\frac{\pi d^2}{4}\ln\frac{D_{\mathrm{cyl}}^2}{D_{\mathrm{cyl}}^2-(D_{\mathrm{blg}}-D_{\mathrm{sh}})^2}+8\mu\frac{L_{\mathrm{blg}}}{D_{\mathrm{blg}}-D_{\mathrm{sh}}}\frac{\pi(D_{\mathrm{blg}}-D_{\mathrm{sh}})^2}{4}\frac{D_{\mathrm{cyl}}^2}{D_{\mathrm{cyl}}^2-(D_{\mathrm{blg}}-D_{\mathrm{sh}})^2}+A_{\mathrm{o}}\ln\frac{A_{\mathrm{o}}}{A_{\mathrm{f}}}+m\pi D_{\mathrm{sh}}\frac{L_{\mathrm{cyl}}}{\sqrt{3}}+8\mu\frac{L_{\mathrm{blg}}+h/2}{D_{\mathrm{cyl}}^2-(D_{\mathrm{blg}}-D_{\mathrm{sh}})^2}\frac{\pi(D_{\mathrm{blg}}-D_{\mathrm{sh}})^2}{4}\frac{D_{\mathrm{cyl}}^2}{D_{\mathrm{cyl}}^2-(D_{\mathrm{blg}}-D_{\mathrm{sh}})^2}\right]$
$F_{LB,1}$: LB without friction from shaft and wall	$F_{\mathrm{LB}}=A_{\mathrm{o}}Y_{\mathrm{o}}\ln\frac{A_{\mathrm{o}}}{A_{\mathrm{f}}}$
$F_{LB,2}$: LB with friction from shaft	$F_{\mathrm{LB},1}=A_{\mathrm{o}}Y_{\mathrm{o}}\ln\frac{A_{\mathrm{o}}}{A_{\mathrm{f}}}+m\pi D_{\mathrm{sh}}\frac{Y_{\mathrm{o}}}{\sqrt{3}}L_{\mathrm{cyl}}$

Table 2 HF2V device parameters.

devices	L_{cyl} (mm)	L_{blg} (mm)	D_{cyl} (mm)	D_{blg} (mm)	D_{shaft} (mm)	α (°)
1	110	30	89	40	30	68.2
2	110	30	89	50	30	51.3
3	110	30	89	58	30	41.8
4	130	30	66	40	30	68.2
5	130	30	66	50	30	51.3
6	50	23.3	50	32	20	56.8
7	70	20	50	32	20	56.3
8	100	30	50	35	24	66.3
9	160	20	60	42	33	62.1
10	100	23	50	35	24	59.9
11	75	30	70	48	30	54.2
12	160	20	54	35	30	73.6
13	160	20	54	36	30	70.6
14	160	20	54	38	30	64.8
15	100	17.2	40	27	20	65.3

begins to flow plastically and is defined as

$$\overline{Y}=\frac{K\varepsilon}{1+n}, \tag{22}$$

where K is the strength coefficient and n is the strain-hardening component. K = 26.4 and n = 0.28 for commercially pure lead [58]. The corresponding calculated Y_{o} values are listed in Table 3. Additionally, ε is the strain during the deformation process, which is defined as follows:

$$\varepsilon=\frac{D_{\mathrm{o}}-D_{\mathrm{f}}}{D_{\mathrm{o}}}, \tag{23}$$

where

$$D_{\mathrm{o}}=\frac{D_{\mathrm{cyl}}-D_{\mathrm{sh}}}{2}\quad\text{and}\quad D_{\mathrm{f}}=\frac{D_{\mathrm{cyl}}-D_{\mathrm{blg}}}{2}. \tag{24}$$

The stress in the lead material is sensitive to purity, strain

Table 3 Shear and yield strength values of pure lead

devices	ε	Y_o (N/mm^2)
1	0.17	25.09
2	0.34	30.47
3	0.47	33.48
4	0.28	28.82
5	0.56	34.99
6	0.40	31.92
7	0.40	31.92
8	0.42	32.42
9	0.33	30.33
10	0.42	32.42
11	0.45	32.99
12	0.21	26.59
13	0.25	27.98
14	0.33	30.33
15	0.35	30.74

rates, strain, and reduction percentages [18,58,59]. The reduction percentage in HF2V devices is the reduction in the area of lead at the bulge's flat surface. The yield stresses calculated for lead using Eq. (21) are comparable to the yield stress values obtained from pure lead compression tests at 20°C for all reduction percentages [59]. The yield strengths derived from the compression and shearing of lead are very similar. Therefore, the yield strength values for lead under compression and shearing are considered to be the same, as shown in Table 3.

The friction factor (m) of 0.866 was calculated using the following relationship [60]:

$$m = 2\mu\sqrt{3}. \tag{25}$$

A total of 15 HF2V experimental device forces (F_{exp}) were compared to the estimated UB and LB forces. Additionally, the UB and LB forces were compared to the peak forces obtained from the experimental tests. The experimental forces should lie between the UB and LB forces [30].

The UB and LB models can provide rough estimates for a broad range of maximum and minimum expected forces for HF2V devices. Obtaining the ratios of model forces to experimental forces provides a convenient comparison that is independent of the scale of a given device. For practical applications, these methods should be helpful for determining the best estimates of device design forces by calculating the averages of the UB and LB models whose force predictions are closest to the corresponding experimental device forces. The variability in the combined model predictions across devices is quantified by using the lognormal standard deviation and lognormal geometric mean of the data to account for the typically skewed distributions of results [61,62].

3 Results and discussion

The experimental HF2V device forces were compared to UB and LB estimates of the forces calculated using the equations listed in Table 1. The results are listed in Table 4 and presented in Fig. 5. For the direct extrusion model, the $F_{UB,2}$ forces are larger and the $F_{LB,1}$ forces are smaller than the experimental forces in all cases, as expected. The $F_{UB,1}$ values are larger than the peak experimental forces for all devices except devices 9 and 15, where the experimental forces are slightly larger than $F_{UB,1}$.

The results of the indirect extrusion model reveal that the UB forces without wall friction ($F_{UB,3}$) are lower than the experimental forces, except for those of devices 12, 13, and 14. However, when considering the wall friction between the lead and cylinder, the UB forces ($F_{UB,4}$) are greater than the experimental forces for all 15 devices.

The LB forces from $F_{LB,1}$ and $F_{LB,2}$ are lower than all the experimental forces. However, the values from $F_{LB,1}$ are excessively low because they neglect the forces from friction. These results demonstrate the significance of friction forces in HF2V devices. Earlier work on extrusion force prediction [12,13] has categorized devices into three groups based on their overall physical dimensions. These results also match the observations in Refs. [12,13] of friction forces contributing between 10% and 60% of the total device forces in typical and large devices.

The UB force values from the direct extrusion analogy are much greater than those calculated by the indirect extrusion models. This can be attributed to the assumption that the entire billet moves through the cylinder with ram displacement [63]. The UB estimates are the largest and have the largest variations relative to the experimental forces for devices 2, 3, and 5, which have the largest bulge and cylinder sizes. Therefore, they shear larger areas of lead and produce more heat, leading to greater variation in experimentally generated forces.

In particular, during repeated cycles, heat is produced in HF2V devices [64,65]. The yield stress values for the same reduction percentages vary with temperature [59] and the lead extrusion pressure has been observed to decrease with an increase in temperature [41,64]. However, temperature variations and/or heat produced during HF2V device experiments have not been measured. The UB forces could be better estimated with knowledge regarding strain percentages, strain rates, and temperature-dependent models for yield value calculations.

It is evident from Fig. 5 that out of the two derived LB models, $F_{LB,2}$ predicts force values that are closer to the actual device forces. Additionally, as expected, the approximated forces from the UB models of $F_{UB,1}$ and $F_{UB,4}$ are greater than the device forces and lie closer to the actual forces. Therefore, for precise device force estimation, a combination of UB and LB models should be considered. The mean predicted force values for each device from $F_{UB,1}$ and $F_{LB,2}$ or the mean values predicted

Table 4 Comparison of estimated HF2V LB and UB forces to experimental forces. UB forces $F_{UB,1–4}$ are ordered from tightest (left) to loosest (right)

devices	$F_{LB,1}$ (kN)	$F_{LB,2}$ (kN)	F_{exp} (kN)	$F_{UB,3}$ (kN)	$F_{UB,4}$ (kN)	$F_{UB,1}$ (kN)	$F_{UB,2}$ (kN)
1	23.5	106.1	205	119.8	290.7	251.6	422.3
2	67.9	168.2	305	232.9	461.0	461.5	677.4
3	114.1	224.3	380	353.0	610.1	677.7	921.4
4	18.4	130.6	175	161.3	297.9	270.1	418.1
5	63.7	199.9	310	284.3	461.1	472.7	667.4
6	23.4	55.3	130	78.7	174.5	151.4	204.9
7	23.4	68.0	150	97.6	184.4	173.1	239.9
8	18.9	96.6	155	129.2	242.1	212.7	304.2
9	14.3	174.1	260	234.7	338.4	327.1	480.1
10	18.9	96.6	155	133.0	227.2	213.6	308.7
11	48.7	122.8	250	175.2	354.3	327.2	431.0
12	5.5	132.9	145	174.8	249.9	238.4	356.6
13	7.0	141.0	165	187.5	265.0	257.2	382.1
14	11.3	156.6	185	213.3	302.6	293.1	429.5
15	8.4	69.7	125	96.1	150.4	143.2	212.1

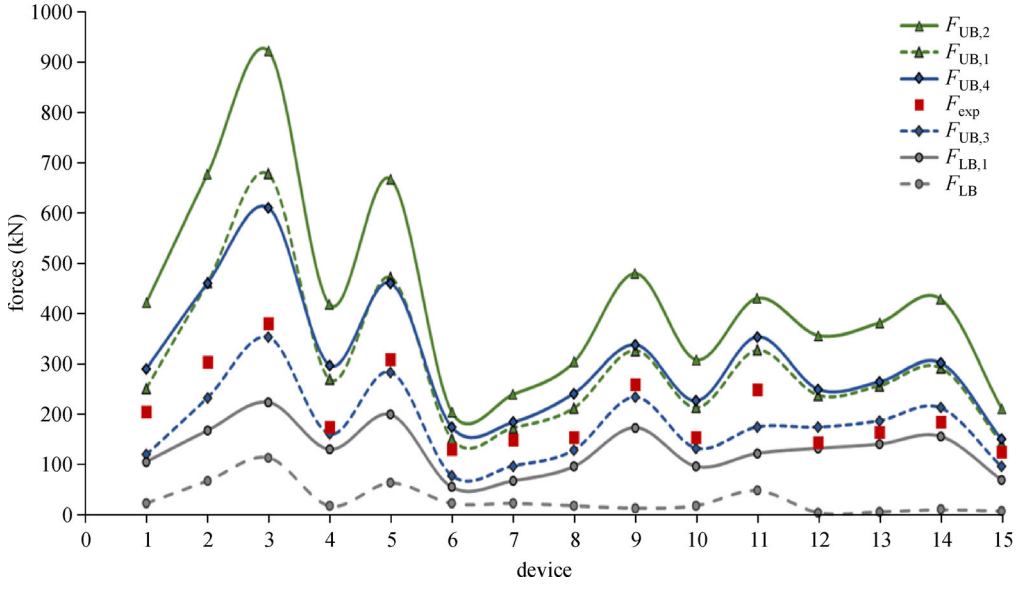

Fig. 5 UB and LB force ranges for HF2V devices.

for each device from $F_{UB,4}$ and $F_{LB,2}$ could be used to provide an improved estimate of approximate HF2V device forces. The ratio of the model forces to the experimental forces is plotted in Fig. 6 (dotted lines). Based on the average ratios of $F_{UB,1}/F_{exp}$ and $F_{LB,2}/F_{exp}$ or $F_{UB,4}/F_{exp}$ and $F_{LB,2}/F_{exp}$, as shown in Fig. 6, the best estimate was determined by assessing the statistical distributions of these outcomes. The lognormal multiplicative standard deviation and lognormal geometric mean of these ratios are listed in Table 5. The lognormal geometric mean of both models is close to 1.0, indicating that the model approximations are close to the experimental device forces. The multiplicative standard deviations of both models exhibit variability under 20%. However, the averages of $F_{UB,4}$ and $F_{LB,2}$ exhibit smaller variability and better model compatibility for the precise calculation of HF2V device forces.

To provide a deeper understanding of the dependency of HF2V device forces and estimated UB and LB forces on device parameters, the 15 devices are plotted in Fig. 7 in terms of increasing values of key HF2V geometric parameters according to previous research [12,13]. The

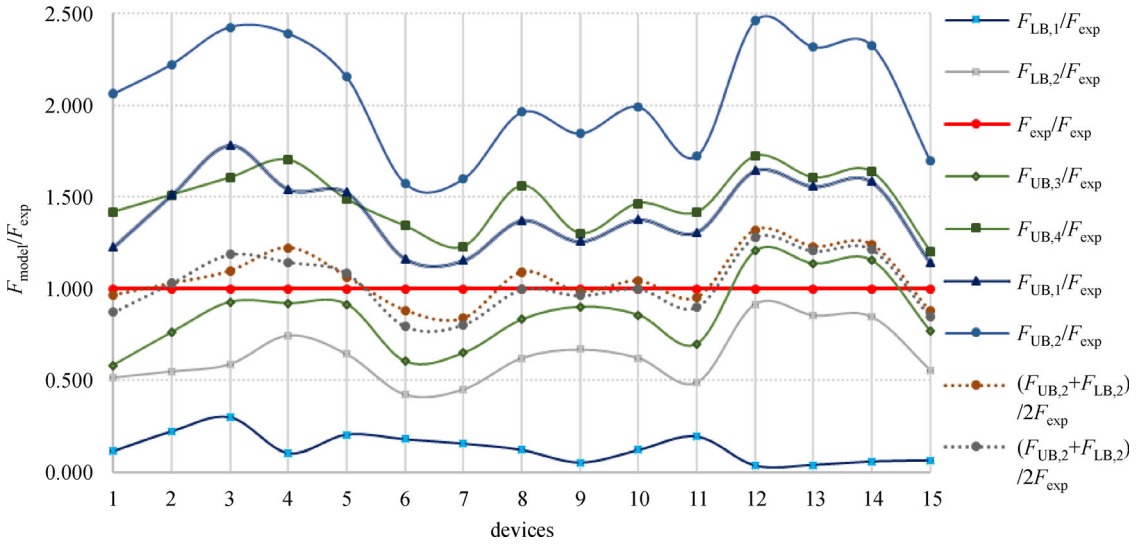

Fig. 6 UB and LB model forces plotted based on F_{model}/F_{exp} and precise device forces calculated (dotted lines) from UB and LB model combinations.

Table 5 Comparison of statistical outcomes of UB-LB combinations for model approximations to experimental results for device force estimation

UB-LB model combinations	mean	median	standard deviation
$\left(\frac{F_{UB,1}}{F_{exp}}+\frac{F_{LB,2}}{F_{exp}}\right)/2$	0.011	1.011	15.7%
$\left(\frac{F_{UB,4}}{F_{exp}}+\frac{F_{UB,1}}{F_{exp}}\right)/2$	0.047	1.048	13.7%

numbers on the plots indicate the numbers of devices used for sorting.

In Fig. 7, when the results are ranked by the value of D_{cyl}, the UB and LB values for all models increase monotonically, excluding those for devices 1, 4, and 11. This result strongly implies that D_{cyl} has a significant influence on overall extrusion force. In particular, the D_{cyl} value broadly determines the volume of lead available for deformation. Therefore, this diameter can be used as a rough indicator of device scale and indicates that larger devices produce more resistive force.

For the devices sorted in increasing order of the projected bulge area *AB*, as shown in Fig. 7, larger *AB* values produce more resistive forces. A larger bulge area *AB* means that more lead can be displaced and sheared by the shaft bulge, thereby producing larger deformation, compressive, and shear forces. This result is intuitive according to basic extrusion theory and provides additional validation for our analysis.

However, the correlation between resistive force and surface area *SA* is unclear. For two devices with the same cross-sectional properties, if one is designed to accommodate additional stroke with a larger D_{cyl}, it may only increase the *SA* and frictional force, and not the extrusion force. Therefore, devices that have design constraints in terms of length can achieve higher force capacities by increasing D_{cyl} or *AB*. Similarly, large devices requiring lower force capacities for larger surface areas can adjust their D_{cyl} and *AB* values to achieve the desired force capacities. Therefore, our UB models can be used as a reference for safely designing HF2V devices within desired force ranges in the future.

However, as discussed previously, our model does not account for heating effects caused by the high amount of shearing that occurs in larger devices, which may lead to a decrease in the flow stress and friction factor, as well as thermal softening [66,67]. Softening, which occurs at room temperature, affects the overall strength of lead [18]. In HF2V devices, the effects of increased temperature are unclear because elevated temperatures decrease overall extrusion forces and accelerate recrystallization, leading to the rapid recovery of plasticity.

However, there is no record of the testing temperatures during the experimental HF2V tests or the heat generated during these device experiments because no temperatures were measured. Measuring the true lead temperature inside an HF2V device would be challenging because a thermocouple placed against the cylinder wall during tests would only measure the temperature of the cylinder wall, not the actual temperature of the lead. Despite the good thermal conductivity of lead and steel, a temperature gradient exists, meaning that an external thermocouple would likely provide an inaccurate indication of the internal lead temperature.

Additionally, the theoretical values obtained from Eqs. (11) and (13) indicate that the flow stress or average flow stress values increase with increasing strain.

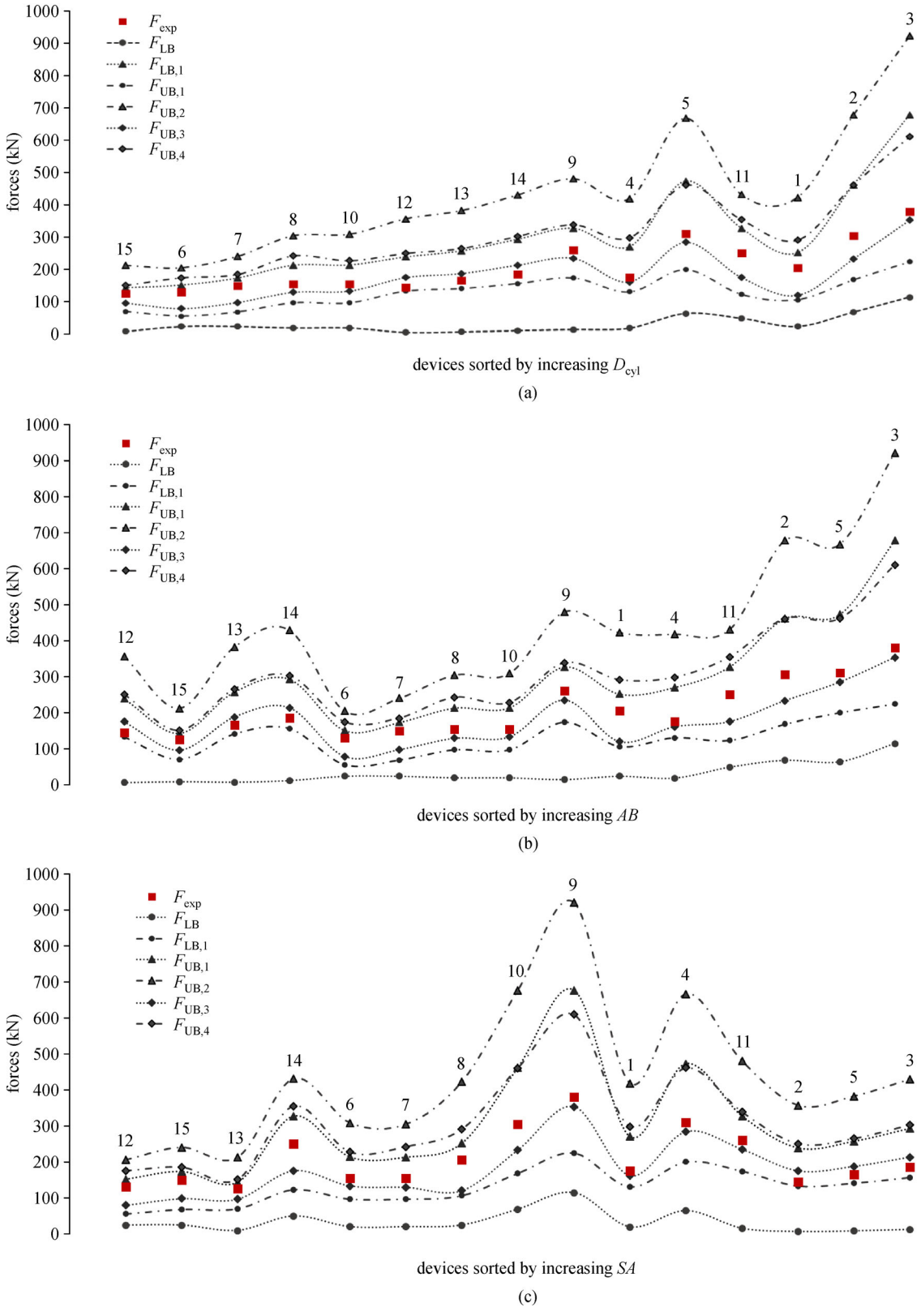

Fig. 7 HF2V forces sorted by key device parameters. (a) Cylinder diameter; (b) bulge area; (c) surface area.

However, it has been experimentally observed that the flow stress and yield strength can remain constant or even decrease after the lead reaches 40% to 50% strain [18,59,68]. Therefore, it is advisable to consider the strain-related effects and strain softening in lead that occur during HF2V extrusion for UB and LB force estimation [20]. More accurate flow stress estimation can be performed using equations considering thermal effects [66,69] or by performing reliable experimental tests on lead properties under various strains and temperatures [59,68], as well as different forms of deformation.

4 Conclusions

The extrusion process in HF2V devices is highly nonlinear based on the material properties, internal mechanics, and geometric conditions inside such devices during motion. This study proposes four analytical UB models and two LB models by extending the analytical mechanics of direct and indirect extrusion force models to match the mechanisms of HF2V devices. The proposed device force models predict forces accurately with all predicted UB forces lying above the experimental forces, excluding the values predicted by $F_{UB,3}$. UB and LB forces limit the operational ranges of HF2V devices based on the device design parameters and deformation of lead within the devices. The averages of the $F_{UB,4}$ and $F_{LB,2}$ values from the UB and LB models approximated the expected HF2V device forces from the UB and LB models with the geometric mean ratio of predicted force to experimental force within 5% of unity across 15 devices with a multiplicative standard deviation of 15.7%. The key device design parameters influencing device forces identified in this study match the findings of previous research. Therefore, these equations can provide useful guidance for future device design to target specific desired force capacities more accurately.

Acknowledgements this project was partially supported by QuakeCoRE, which is a center funded by the New Zealand Tertiary Education Commission. This is QuakeCoRE publication number 0623.

References

1. Geller R J. Earthquake prediction: A critical review. Geophysical Journal International, 1997, 131(3): 425–450
2. Ouzounov D, Pulinets S, Hattori K, Taylor P. Pre-earthquake processes: A multidisciplinary approach to earthquake prediction studies. International Geology Review, 2019, 61(16): 2080–2082
3. Zhang Y, Wu Z, Zhang X. Annual Earthquake Potential Consultation: A Real Forward Prediction Test in China, in Earthquake and Disaster Risk: Decade Retrospective of the Wenchuan Earthquake. Singapore: Springer, 2019, 117–134
4. Skinner R I, Tyler R G, Heine A J, Robinson W H. Hysteretic dampers for the protection of structures from earthquakes. Bulletin of the New Zealand National Society for Earthquake Engineering, 1980, 13(1): 22–36
5. Rodgers G W, Chase J G, Mander J B, Leach N C, Denmead C S. Experimental development, tradeoff analysis and design implementation of high force-to-volume damping technology. Bulletin of the New Zealand Society for Earthquake Engineering, 2007, 40(2): 35–48
6. Robinson W H. US Patent, 6,220,410 B1. 2001
7. Robinson W H. US Patent, 4,117,637. 1978
8. Robinson W H, Greenbank L R. An extrusion energy absorber suitable for the protection of structures during an earthquake. Earthquake Engineering & Structural Dynamics, 1976, 4(3): 251–259
9. Cousins W J, Porritt T E. Improvements to lead-extrusion damper technology. Bulletin of the New Zealand National Society for Earthquake Engineering, 1993, 26(3): 342–348
10. Rodgers G W, Mander J B, Chase J G, Dhakal R P, Leach N C, Denmead C S. Spectral analysis and design approach for high force-to-volume extrusion damper-based structural energy dissipation. Earthquake Engineering & Structural Dynamics, 2008, 37(2): 207–223
11. Parulekar Y M, Reddy G R, Vaze K K, Kushwaha H S. Lead extrusion dampers for reducing seismic response of coolant channel assembly. Nuclear Engineering and Design, 2004, 227(2): 175–183
12. Vishnupriya V, Rodgers G W, Mander J B, Chase J G. Precision design modelling of HF2V devices. Structures, 2018, 14: 243–250
13. Vishnupriya V, Rodgers G W, Chase J G. Precision design modelling of HF2V devices. In: New Zealand Society of Earthquake Engineering Annual Conference (NZSEE 2017) and the Anti Seismic Systems International Society (ASSISI) 15th World Conference on Seismic Isolation, Energy Dissipation and Active Vibration Control of Structures. Wellington, 2017
14. Latham D, Reay A M, Pampanin S. Kilmore street medical centre: Application of a post-tensioned steel rocking system. In: Steel Innovations Conference 2013. Christchurch, 2013
15. Latham D A, Reay A M, Pampanin S. Kilmore street medical centre: Application of an advanced flag-shape steel rocking system. In: New Zealand Society for Earthquake Engineering–NZSEE–Conference. Wellington, 2013
16. Abe H, Ichihashi I, Kuroda K, Iwatsubo T, Ta K. Seismic proving test of heavy component with energy absorbing support. In: Proceedings of the International Conference on Global Environment and Advanced Nuclear Power Plants. Kyoto: 2002, 107–111
17. Iwatsubo T, Sasaki Y, Abe H, Kuroda K, Saito Y, Tai K, Sumiya H. NUPEC project: Seismic proving test of heavy component with energy absorbing support. In: 7th International Conference on Nuclear Engineering. Tokyo, 1999
18. Hofmann W. Lead and Lead Alloys. Berlin, Heidelberg: Springer, 1970
19. Rodgers G W. Next generation structural technologies: Implementing high force-to-volume energy absorbers. Dissertation for the Doctoral Degree. Christchurch: University of Canterbury, 2009
20. Saha P K. Aluminum Extrusion Technology. Ohio: ASM International, Materials Park, 2000
21. Chen C, Ling F. Upper-bound solutions to axisymmetric extrusion problems. International Journal of Mechanical Sciences, 1968,

10(11): 863–879
22. Adie J, Alexander J. A graphical method of obtaining hodographs for upper-bound solutions to axi-symmetric problems. International Journal of Mechanical Sciences, 1967, 9(6): 349–357
23. Drucker D, Prager W, Greenberg H. Extended limit design theorems for continuous media. Quarterly of Applied Mathematics, 1952, 9(4): 381–389
24. Hosford W, Caddell R. Mechanics and Metallurgy. Cambridge: Cambridge University Press, 2007
25. Rowe G W. Elements of Metalworking Theory. London: Hodder Arnold, 1979
26. Kudo H. An upper-bound approach to plane-strain forging and extrusion—III. International Journal of Mechanical Sciences, 1960, 1(4): 366–368
27. Chen P C. Upper bound solutions to plane-strain extrusion problems. Journal of Engineering for Industry, 1970, 92(1): 158–164
28. Hashmi M. A lower bound solution for the plane strain extrusion forging process. Mathematical and Computer Modelling, 1988, 11: 1183–1188
29. Oluwole O, Adewumi A. Comparative analysis of analytical and graphical upperbound solutions for 4-high reversing aluminium cold-rolling sheet mill. Science and Technology, 2012, 2(1): 30–36
30. Avitzur B, Bishop E D, Hahn W C Jr. Impact extrusion—Upper bound analysis of the early stage. Journal of Engineering for Industry, 1972, 94(4): 1079–1086
31. Tiernan P, Hillery M T, Draganescu B, Gheorghe M. Modelling of cold extrusion with experimental verification. Journal of Materials Processing Technology, 2005, 168(2): 360–366
32. Pop M, Frunza D, Neag A. Experimental and numerical aspects regarding lead alloy plastic deformation. Romanian Journal of Technical Sciences Applied Mechanics, 2012, 57(1): 71–82
33. Pop M, Frunza D, Neag A, Pavel C. Researches on forward extrusion of lead alloy. Metalurgia, 2012, 64(1): 10
34. Socaciu T. An analysis regarding the variation of necessary force by the indirect extrusion processes. Procedia Technology, 2014, 12: 433–438
35. Ajiboye J S. Upper bound analysis of extrusion from square billets through circular and square/rectangular dies. Journal of Mechanical Science and Technology, 2009, 23(2): 461–474
36. Ebrahimi M, Tiji S N, Djavanroodi F. Upper bound solution of equal channel forward extrusion process as a new severe plastic deformation method. Metallurgical Research & Technology, 2015, 112(6): 609
37. Samanta S. A new die profile with high process efficiency. Applied Scientific Research, 1972, 25(1): 54–64
38. Yang D Y, Han C H. A new formulation of generalized velocity field for axisymmetric forward extrusion through arbitrarily curved dies. Journal of Manufacturing Science and Engineering, 1987, 109(2): 161–168
39. Lee B, Keum Y, Wagoner R. Modeling of the friction caused by lubrication and surface roughness in sheet metal forming. Journal of Materials Processing Technology, 2002, 130–131: 60–63
40. Yoo S S, Kim D E. Minimum lubrication technique using silicone oil for friction reduction of stainless steel. International Journal of Precision Engineering and Manufacturing, 2013, 14(6): 875–880
41. Zhou Y. Lead 65: Edited Proceedings, Second International Conference on Lead. Arnhem: Elsevier Science, 2014
42. Bowden F P, Leben L. The nature of sliding and the analysis of friction. Proceedings of the Royal Society of London. Series A, Mathematical and Physical Sciences, 1939, 169(938): 371–391
43. Symons D D, Chen J, Alton P. Calculation of optimal jaw geometry for an electronic bond pull test. Proceedings of the Institution of Mechanical Engineers. Part C, Journal of Mechanical Engineering Science, 2014, 228(11): 1847–1858
44. Horrobin D, Nedderman R. Die entry pressure drops in paste extrusion. Chemical Engineering Science, 1998, 53(18): 3215–3225
45. Groover M P. Principles of Modern Manufacturing: SI Version. Hoboken, NJ: Wiley & Sons, 2013
46. Pradip K. Aluminum Extrusion Technology. Ohio: ASM International, 2000
47. Hora P, Becker C, Tong L C, Maier J, Müller S. Advanced frictional models for extrusion application. Key Engineering Materials, 2014, 585: 41–48
48. Hsu T C, Huang C C. The friction modeling of different tribological interfaces in extrusion process. Journal of Materials Processing Technology, 2003, 140(1–3): 49–53
49. Bakhshi-Jooybari M. A theoretical and experimental study of friction in metal forming by the use of the forward extrusion process. Journal of Materials Processing Technology, 2002, 125–126: 369–374
50. Ma X, De Rooij M B, Schipper D J. Modelling of contact and friction in aluminium extrusion. Tribology International, 2010, 43(5–6): 1138–1144
51. Liu Y F, Li J, Zhang Z M, Hu X H, Zhang W J. Experimental comparison of five friction models on the same test-bed of the micro stick-slip motion system. Mechanical Sciences, 2015, 6(1): 15–28
52. Dongare V S. Hot Extrusion of Carbon Nanotube-Magnesium Matrix Composite Wire. Ohio: Ohio University, 2014
53. DePierre V, Gurney F. A method for determination of constant and varying friction factors during ring compression tests. Journal of Lubrication Technology, 1974, 96(3): 482–487
54. Velu R, Cecil M. Quantifying interfacial friction in cold forming using forward rod backward cup extrusion test. Journal of The Institution of Engineers (India): Series C, 2012, 93(2): 157–161
55. Hosford W F, Caddell R M. Metal Forming: Mechanics and Metallurgy. Cambridge: Cambridge University Press, 2011
56. Rodgers G W, Solberg K M, Chase J G, Mander J B, Bradley B A, Dhakal R P, Li L. Performance of a damage-protected beam-column subassembly utilizing external HF2V energy dissipation devices. Earthquake Engineering & Structural Dynamics, 2008, 37(13): 1549–1564
57. Wrzesniak D, Rodgers G W, Fragiacomo M, Chase J G. Experimental testing of damage-resistant rocking glulam walls with lead extrusion dampers. Construction & Building Materials, 2016, 102: 1145–1153
58. Wong S, Hodgson P D, Thomson P F. Room temperature deformation and recrystallisation behaviour of lead and lead–tin alloys in torsion and plane strain compression. Materials Science and Technology, 1999, 15(6): 689–696
59. Loizou N, Sims R B. The yield stress of pure lead in compression. Journal of the Mechanics and Physics of Solids, 1953, 1(4): 234–

243

60. Molaei S, Shahbaz M, Ebrahimi R. The relationship between constant friction factor and coefficient of friction in metal forming using finite element analysis. Iranian Journal of Materials Forming, 2014, 1(2): 14–22
61. Solberg K, Mander J, Dhakal R. A rapid financial seismic risk assessment methodology with application to bridge piers. In: The 19th Australasian Conference on Mechanics of Structures and Materials (ACMSM19). Christchurch: Progress in Mechanics of Structures and Materials, 2006
62. Limpert E, Stahel W A, Abbt M. Log-normal distributions across the sciences: Keys and clues: on the charms of statistics, and how mechanical models resembling gambling machines offer a link to a handy way to characterize log-normal distributions, which can provide deeper insight into variability and probability—Normal or log-normal: that is the question. Bioscience, 2001, 51(5): 341–352
63. Sheppard T, Tunnicliffe P, Patterson S. Direct and indirect extrusion of a high strength aerospace alloy (AA 7075). Journal of Mechanical Working Technology, 1982, 6(4): 313–331
64. Rodgers G W, Chase J G, Heaton D, Cleeve L. Testing of lead extrusion damping devices undergoing representative earthquake velocities. In: New Zealand Society for Earthquake Engineering (NZSEE) Annual Technical Conference. Wellington: NZSEE Conference Publication, 2013
65. Patel C C. Seismic analysis of parallel structures coupled by lead extrusion dampers. International Journal of Advanced Structural Engineering, 2017, 9: 177–190
66. Yadav S, Repetto E A, Ravichandran G, Ortiz M. A computational study of the influence of thermal softening on ballistic penetration in metals. International Journal of Impact Engineering, 2001, 25(8): 787–803
67. Flitta I, Sheppard T. Nature of friction in extrusion process and its effect on material flow. Materials Science and Technology, 2003, 19(7): 837–846
68. Tober G, Anopuo O, Maier P. Lead as test rolling material for hot complex rolling of steel. Advanced Materials Research, 2012, 428: 84–88
69. DeLo D, Semiatin S. Finite-element modeling of nonisothermal equal-channel angular extrusion. Metallurgical and Materials Transactions. A, Physical Metallurgy and Materials Science, 1999, 30(5): 1391–1402